

Comparison of SfM Computer Vision Point Clouds of a Landslide Derived from Multiple Small UAV Platforms and Sensors to a TLS based Model

Samantha Ruggles, Joseph Clark, Kevin W. Franke, Derek Wolfe, Brandon Reimschiessel, R. Abraham Martin, Trent J. Okeson, and John D. Hedengren

Abstract: Structure from motion (SfM) computer vision is a remote sensing method that is gaining popularity due to its simplicity and ability to accurately characterize site geometry in three dimensions (3D). While many researchers have demonstrated the potential for SfM to be used with unmanned aerial vehicles (UAVs) to model in three dimensions various geologic features such as landslides, little is understood how the selection of the UAV platform can affect the resolution and accuracy of the model. This study evaluates the resolution and accuracy of 3D point cloud models of a large landslide that occurred in 2013 near Page, Arizona that were developed from various small UAV platform and camera configurations. Terrestrial laser scans (TLS) were performed at the landslide and were used to establish a comparative baseline model. Results from the study indicate that point cloud resolution improved by more than 16% when using multi-rotor UAVs instead of fixed-wing UAVs. However, accuracy of the points in the point cloud model appear to be independent of the UAV platform, but depend principally on the selected camera and the image resolution. Additional practical guidance on flying various UAV platforms in challenging field conditions is provided for geologists and engineers.

Key words: UAV, computer vision, structure from motion, landslide, terrestrial laser scanning.

1. Introduction

Interest in and demand for remote sensing using small unmanned aerial vehicles (sUAVs, or “drones”) is increasing rapidly throughout the world. With these systems becoming more affordable and user-friendly, sUAV-related research has become accessible to a wider range of engineers and Earth scientists. In particular, the fields of civil engineering and engineering geology are showing substantial interest in sUAV-related applications of remote sensing, infrastructure monitoring, and post-hazard damage assessment. For example, researchers have experimented with sUAVs to remotely collect data related to soil erosion (D’Oleire-Oltmanns et al. 2012; Kaiser et al. 2014), landslide and rock fall deformations (Gong et al. 2010; Lucieer et al. 2014; Niethammer et al. 2012; Stumpf et al. 2013; Turner et al. 2015), traffic monitoring (Coifman et al. 2006; Zhou et al. 2015), road surface distress (Dobson et al. 2013; Zhang and Elaksher 2012), geological and/or topographical terrain mapping (Bemis et al. 2014; Stefanik et al. 2011), coastal monitoring (Harwin and Lucieer 2012; Mancini et al. 2013), bridge monitoring (Metni and Hamel 2007), earthwork and site grading (Siebert and Teizer 2014), pipeline monitoring (Hausamann et al. 2005; Rathinam et al. 2008), and levee monitoring (de Al-

buquerque Nóbrega et al. 2013). Some research has been performed with sUAVs to obtain site data following a major earthquake including evaluations of seismically-induced landslide displacements (Gong et al. 2010), structural transportation damage detection (Hu et al. 2012), and post-liquefaction evaluation of ground deformations (Ledezma 2014).

While some of these cited studies used various remote sensing technologies such as stereo vision (Stefanik et al. 2011) or synthetic aperture radar (SAR) (de Albuquerque Nóbrega et al. 2013) to collect and analyze their respective datasets, the majority of the studies applied a remote sensing technique known as structure from motion (SfM) computer vision (Marr and Nishihara 1978; Snavely et al. 2008). Continual advances in digital photography, computer processing capabilities, and computer vision algorithms have improved the speed and accuracy of SfM computer vision such that median accuracies as high as 2.5 cm have recently been reported in the literature for sUAV-based SfM digital terrain models (DTMs) (Harwin and Lucieer 2012). Even low-cost sUAV platforms carrying very small and affordable sensors are commonly producing SfM-based DTMs with accuracies of 0.5-meter or better (Niethammer et al. 2012; Stumpf et al. 2013).

While a DTM accuracy of 0.5-meter might be sufficient for many engineering and science applications, it may not be sufficient for other applications that require higher accuracy. For example, detection of post-earthquake liquefaction ground deformations might require horizontal model accuracies within 10 cm and vertical model accuracies within 1 cm to be of use to the engineering community. Experts in the field of remote sensing generally understand that various methods can be employed to improve resolution and/or accuracy of SfM 3D reconstructions including the use of a higher-quality camera and/or computer workstation for SfM processing, increasing

Samantha Ruggles, Joseph Clark, Kevin W. Franke,¹ and Derek Wolfe. Dept. of Civil and Environ. Eng., Brigham Young Univ., Provo, UT 84602

Brandon Reimschiessel. Dept. of Elec. and Comp. Eng., Brigham Young Univ., Provo, UT 84602

R. Abraham Martin, Trent J. Okeson, and John D. Hedengren. Dept. of Chemical Eng., Brigham Young Univ., Provo, UT 84602

¹Corresponding author (e-mail: kevin_franke@byu.edu).

the number of pixels per surface area in each digital image, incorporating GPS and/or telemetry metadata with the digital images, and/or incorporating surveyed ground control points in the SfM workflow. However, the selection of a particular camera and how it is maneuvered at a given site depends largely upon the capabilities of the sUAV platform that is being used. Unfortunately, practical guidance on how different sUAV platform/sensor combinations can affect the final resolution, accuracy, and visual quality of a SfM 3D reconstruction is not readily available to engineers and scientists. Furthermore, studies reported in the literature such as those cited above rarely address this lack of guidance because they tend to collect their respective datasets using a single preferred sUAV platform/sensor combination. As a result, some scientists and engineers might be left wondering which sUAV platform/sensor combination would be best suited for a particular monitoring or research application. Even worse, some engineers and scientists who are unfamiliar with the challenges and/or practical limitations associated with SfM-based remote sensing from an sUAV might adopt the philosophy that selection of an sUAV platform/sensor combination is inconsequential. These professionals might subsequently base the selection of a platform/sensor combination on other factors such as advertised automated flight functionalities, size/portability, perceived convenience, and/or cost instead of the desired final quality, resolution, and/or accuracy of the SfM 3D reconstruction.

Given the general lack of guidance in the literature for engineers and scientists regarding the selection of a sUAV platform/sensor combination, the objectives of this study were to: (1) assess how different sUAV platform/sensor combinations would affect the final resolution, accuracy, and visual quality of an sUAV-based SfM 3D reconstruction and (2) provide practical guidance to engineers and scientists desiring to acquire a sUAV platform/sensor combination for remote sensing field applications. To perform this study, three sUAV platform/sensor combinations were selected and tested at a field site to evaluate two questions: (1) “Does the selection of the optical sensor matter?” and (2) “Does the selection of the sUAV platform type matter?” Two of the selected sUAV platforms represented different multi-rotor types, but that were capable of carrying different-sized optical sensors. Two of the selected sUAV platforms carried the same small optical sensor, but represented platform types that fly in a different manner (i.e., multi-rotor versus fixed wing flight). The selected field site for this study was a large landslide that occurred in 2013 in the State of Arizona in the United States and that severely damaged a major highway. This landslide was selected for the study because of its unique interest to both civil engineers and earth scientists, and because sufficient measurements and controls were already in place at the time of the study so as to provide a meaningful baseline for the SfM model comparisons.

2. Study Area

On February 20, 2013, approximately 32 km south of Page, Arizona, US Highway 89 (US-89) experienced landslide movement that displaced nearly 150 meters of travel lanes (McCormick and Richmond 2013). Vertical scarp displacements of nearly two meters were observed in the travel lanes. The landslide failure surface extended through the road and down

through the entire hillside (see Figure 1). The highway was immediately closed following the landslide, and geotechnical engineers and geologists were brought on-site to assess the damage of the natural disaster, to monitor any continuing movements of the slide, and to propose mitigation solutions.

Fig. 1. sUAV photograph of the US-89 Arizona landslide that occurred on February 20, 2013.



According to Kleinfelder (McCormick and Richmond 2013), the landslide was a reactivated portion of a larger, ancient translational (i.e., planar) landslide. The active landslide is up to approximately 41 m deep below the roadway and measures approximately 370 m long at the base (toe) of the slope. The ancient landslide is approximately 91 m deep and up to 760 m wide (as measured longitudinally along the US-89 highway). While many slope failures are associated with the presence of water, no evidence of groundwater seepage was identified in any of the subsurface explorations. It was therefore concluded that the 2013 landslide occurred under dry conditions due to long-term slope creep and slow but continual erosion at the base of the slope. Kleinfelder suggested that the slope would continue to move if action was not taken to mitigate the landslide, and proposed that the most feasible mitigation option was the construction of a gravity buttress at the base of the landslide slope, and the realignment of the highway travel lanes further back into the rock slope through the creation of a new back cut. This concept would move the highway away from the headscarp of the landslide and would provide the needed fill materials to construct the buttress at the base of the slope. The State of Arizona proceeded to implement the geotechnical engineering recommendations of Kleinfelder (McCormick and Richmond 2013) in summer 2014, completing the construction in 2015.

3. Methods

This study compares a baseline terrestrial laser scan (TLS) model of the US-89 landslide with corresponding SfM computer vision models developed from digital photographs taken with three different sUAV platform/sensor combinations. The photographs and laser scans were captured during the same two-day period during July 2014 that the TLS scans were performed at the landslide site. The sUAV platform/sensor combinations used in this study were carefully selected to represent generic types of sUAV platform/sensor combinations that are commercially available to engineers and scientists and are

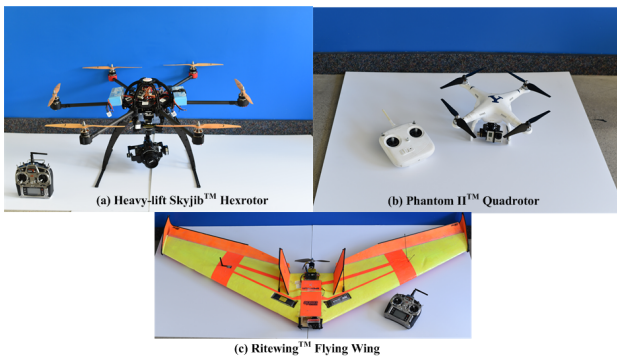
commonly used. This section describes how these sUAV platforms were selected and operated, how the digital images were collected with the selected sensors, and the SfM workflow with which those images were processed to develop 3D reconstructions of the landslide. This section also describes the collection of the TLS data used as the basis for model comparisons (i.e., ground truth) in this study.

3.1. Selected sUAV Platforms

For this study, three platforms were selected to represent three generic types of sUAV platforms that are currently popular with engineers and scientists. Consideration was given to select: (1) two of the three platform types that had similar flight capabilities, but that could carry different optical sensors, and (2) two of the three platform types that could carry the same optical sensor, but that had different flight capabilities. The selected sUAV platforms included a heavy-lift hexrotor platform, a small quadrotor platform, and a fixed wing platform. Photographs of the selected sUAV platform/sensor combinations used in this study are presented in Fig. 2, and select technical specifications for the three sUAV platforms are provided in Table 1. A single rotor sUAV platform (i.e., helicopter) was not selected for use in this particular study because such platforms are not as widely used as multi-rotor platforms, possibly due to the increased difficulty in piloting them. We also felt that the image sets collected from the heavy-lift multi-rotor/DSLR combination would closely resemble the image sets that would be collected from a heavy-lift single-rotor sUAV platform. However, as will be discussed below, the selection of a single-rotor heavy-lift sUAV platform would likely have overcome some of the environmental difficulties that were eventually encountered at the desert landslide.

In practice, each individual sUAV platform will have its own unique automation/navigation features, payload/duration characteristics, and customizable upgrade options. Engineers and scientists should carefully evaluate each sUAV platform and its capabilities before purchasing to ensure that it will provide all of the necessary and/or desired features for its intended mission(s) (Coopmans 2014; Stark et al. 2012).

Fig. 2. Photographs of the three different sUAV platforms used in this study.



3.2. sUAV Flight Patterns

Each of the three selected sUAV platform/sensor combinations was flown manually over the US-89 landslide for suffi-

cient duration to collect approximately 600 aerial digital photographs of the landslide, excluding images captured during take-off and landing. Because the average flight time per battery charge on each sUAV used in this study was about 12 minutes, each sUAV was flown three times to ensure adequate aerial coverage and image overlap at the landslide. For the study, all sUAV platforms were manually piloted using first person view (FPV) navigation technology, and line-of-sight vision of the sUAV was maintained at all times. A spotter assisted the sUAV operator as needed.

The flight path implemented for all three sUAV platforms followed a systematic back-and-forth pattern at elevations of 10, 30, 60, and 120 meters above the landslide. The purpose of this flight pattern was to collect numerous images from multiple viewing angles and elevations to improve image overlap and resolution, resulting in improved quality of the 3D reconstructions. These photos had a side overlap that ranged from 70% to 90% depending on the elevation of the pass and front to back overlap greater than 80% for each of the platforms. In total, each sUAV collected optical data from the air for approximately 36 minutes over the landslide.

Afternoon desert winds and temperatures exceeding 43° Celsius (i.e., 110° Fahrenheit) caused hexarotor platform to malfunction and fly poorly, elevating the risk of a crash. Specifically, the Electronic Speed Control (ESC) was overheating. At temperatures above 145° Fahrenheit, the ESC would shut down to prevent a fire. On the other hand, the flying wing platform was minimally impacted by the wind and the temperatures. As a result, all multi-rotor sUAV flights were performed in the morning hours before 10:30am, resulting in some undesired shadows in the digital photographs. However, the SfM workflow that was incorporated did not seem to be adversely impacted by the shadows in the photographs, as will be subsequently shown in the model results. Furthermore, this observation of poor multi-rotor sUAV platform performance in high winds and/or elevated temperatures effectively illustrates the importance of selecting an sUAV platform that is capable of performing its remote sensing mission(s) in the intended environment. In hindsight, use of a heavy-lift single-rotor sUAV platform would have likely been a better choice for this particular study if a sufficiently skilled pilot could be found because the large polar moment of inertia of a single spinning rotor would have caused the platform to have much more stability in the afternoon desert winds. However, this solution is impractical on a large scale due to the difficulties of piloting a single rotor UAV. A larger heavy lift multirotor platform with installed cooling systems would be a more feasible solution to overcome the desert winds.

3.3. Selected Sensors

Because sUAVs generally have relatively small payload capacities, one of the most important considerations in selecting onboard sensors is weight. In addition to the weight of the sensor itself, engineers and scientists must also account for the weight of the stabilizing gimbal (if any) and power supply. Thus, smaller UAVs are generally limited to lightweight (i.e., < 700 grams) compact sensors. A heavy-lift multi-rotor sUAV generally has a much larger payload capacity (i.e., > 3 kg).

Two different optical sensors were used in this study. A GoPro® Hero 3+ camera was used with both the Quadrotor and the Fly-

Table 1. Selected sUAV platforms for the landslide study and their specifications.

Category	Platform	Payload	Gimbal	Max Flight Time
Heavy-lift Hexrotor	Aeronavics SkyJib Super-6 Ti-QR	3-5 kg	2-Axis	12-15 min
Quadrotor	DJI Phantom™ II	500 g	2-Axis	15-25 min
Flying Wing	Ritewing™ 8" Zephyr XL	1-2 kg	N/A	20-30 min

ing Wing sUAVs, and a Nikon® D7100 DSLR camera was used with the Hexrotor sUAV. Each of these sensors and their corresponding settings are briefly described below.

3.3.1. GoPro Hero 3+ Camera

The GoPro Hero series of cameras are lightweight, compact cameras designed for reliable operation in extreme environments. The GoPro camera used in this study is capable of 1440p high definition (HD) video (2.7 megapixels (MP)/frame) at 48 frames per second, as well as capturing still images with resolutions as large as 12 MP. Because the sensor weighs only 74 grams, it can be easily carried by almost any sUAV platform that is currently commercially available.

One disadvantage associated with many small sporting cameras such as the GoPro is their use of an ultra-wide angle (or “fish-eye”) lens. Such a lens causes curvature and distortion in SfM 3D reconstruction unless the images are first modified to correct for wide-angle distortion, or the SfM algorithm is calibrated to compensate for the distortion during image processing. Rather than perform these corrections, a commercially customized 5.4mm flat lens was fitted to the GoPro Hero 3+ camera used in this study. It was verified that the new lens had minimal distortion with imagery of lens distortion grids. The resulting GoPro images produced ground sample distances (GSDs) shown in Table 2.

Because the GoPro sensor also provided FPV navigation technology for the sUAV operator in this study, it could not be used to collect still images without disrupting the operator’s view. However, 1440p HD video was collected with the sensor during FPV operation with a shutter speed of 1/48 seconds, with still images later being extracted as part of the SfM processing workflow. Using extracted video images resulted in lower image resolutions (~2.76 MP). Nevertheless, these images were sufficient for performing 3D reconstruction, but produced lower quality models (as will subsequently be shown). Because many commercial sUAV platforms that use GoPro or equivalent sensors incorporate FPV navigation technology, these lower-resolution images effectively simulate the types of images that many practicing engineers and scientists might collect from the field when relying upon FPV to navigate their sUAV platforms.

3.3.2. Nikon D7100 DSLR Camera

The Nikon D7100 DSLR camera used in this study features a 23.5 mm by 15.6 mm DX-format sensor capable of capturing images at resolutions of 24.1 MP with an ISO as low as 100. The camera supports GPS tagging of the images, and can be remotely controlled via a Micro-USB port. The lens used in this study was a Nikon AF-S Nikor 35mm 1:1.8G. This lightweight, fixed-focal length lens has a large aperture, and it does not generate any significant wide-angle or telephoto distortion. The computed GSDs for the D7100 images are shown in Table 2.

Still .JPG images at a resolution of 24.1 MP were captured at a frequency of every 3 seconds. While .RAW image formats are generally considered preferable for SfM processing due to reduced noise and compression, .JPG images were used in this study to be consistent with the GoPro image format and to reduce the necessary SfM processing time. All other functions on the camera were set to their respective “Automatic” settings to imitate what would most likely be used by engineers and scientists in the field. This resulted in a mean shutter speed of 1/175 seconds with speeds ranging from 1/125 seconds to 1/320 seconds.

Table 2. Selected cameras GSD at various elevations above the highway surface ignoring motion effects.

UAV Elevation (m)	Ground Sample Distance (cm/pixel)	
	GoPro	Nikon
10	0.51	0.07
30	1.53	0.22
60	3.07	0.45
120	6.13	0.90

3.4. Baseline LiDAR Data

To enable quantification of 3D point cloud accuracy, as well as meaningful comparisons between different sUAV point clouds, it was necessary to establish an industry-standard point cloud to serve as a baseline for the study. A TLS survey was performed at the landslide during the sUAV flights. For redundancy, two separate TLS scanners were used to gather data from the site: a FARO® Focus^{3D} 130 and a FARO Focus^{3D} 330. Both of these scanners are rated for +/-2mm accuracy to ranges of 130m and 330m, respectively. With the assistance of professional land surveyors, the TLS scanners were placed in a series of pre-determined positions designed to promote maximum coverage of the landslide study area. Several spherical Styrofoam targets with diameters ranging from 150mm to 200mm were placed in the scan vicinity to facilitate object registration (Mancini et al. 2013; Niethammer et al. 2012; Travelletti et al. 2012). In total, 51 separate TLS scans were made using both scanners. All of the TLS scans of the landslide required approximately 32 man-hours to complete due to the steep, boulder-strewn terrain at the site.

Registration of the TLS scans was performed using AutoDesk® *ReCap* software (aut), unifying the scans into a single 3D point cloud model. This model was converted into an .E57 file format, a compressed format compatible with *CloudCompare*, v2.6.1 software (Girardeau-Nontaut), which was later used to perform comparisons between the various 3D point clouds. Overall, the resulting TLS baseline point cloud provided a resolution of over 90,400 points per square meter (i.e., one point per square 1.1 mm). An image of the TLS point cloud model is presented in Figure 3. The shadowing effect caused by concrete highway

barrier is evident in Figure 3 by the large hole of data (shown in white) just above the headscarp of the landslide.

Fig. 3. TLS point cloud model of the US-89 landslide.



No ground control points were surveyed or marked as part of this study because the sUAV-based point cloud models did not require geo-referencing (i.e., latitude, longitude, elevation) for comparisons with the TLS baseline point cloud model. Furthermore, the performance of manual site surveys and the establishment of ground control points are not conducive to many sUAV-based remote sensing applications, including the monitoring of potentially dangerous geological hazard sites such as active rock falls or unstable landslides. Finally, the addition of ground control points would most likely only serve to improve the accuracy of the sUAV-based point cloud models. Given these considerations, ground control points were excluded from this study.

3.5. Standard Boxes

To help ensure model quality, both qualitatively and quantitatively, a series of boxes of known dimensions were placed along the roadway. The smallest box measured 7.6 x 7.6 x 30.5 cm and the largest box was 30.5 x 30.5 x 30.5 cm. The series of boxes would be constant throughout each dataset and preserve geometry in 3 dimensions. The boxes could be measured virtually and compared to true dimensions to check for model accuracy and help produce a reliable scale factor. Due to the fact that the analysis software does not function properly with global coordinates and because GPS GCPs (ground control points) were not available for this case study, the boxes served as reference points that could be used for dimensioning and as anchor points for manual alignment of the point clouds before iterative closest point (ICP) (Besl and McKay 1992) algorithm could take place. After each model was generated it was easy to tell how aesthetic and detailed the models were by looking at the boxes and seeing if geometry was preserved and if the numbering on the boxes was easily legible. Figure 4 presents an aerial photograph of these boxes and their layout on the highway pavement.

3.6. Processing

The computer workstation used to perform the SfM model processing in this study was a customized machine with the following specifications:

- Intel® Core i7-4770 CPU @ 3.40 GHz
- 32GB DDR Random Access Memory (RAM)

Fig. 4. Aerial photograph of 12 wooden boxes placed along the highway for reference and comparison.



- nVidia® GeForce GTX 780 Ti graphics card

This computer workstation was adequate to process the multiple sets of sUAV-based image to develop the various SfM 3D reconstructions. The image sets from each sUAV/sensor combination were generally able to be processed within 24 hours. However, we have observed that most commercial SfM algorithms will utilize all of the computer processing power that is available, and that the meshing and viewing of large 3D models is typically best if performed with at least 60 GB of RAM.

3.7. Computer Vision and 3D Reconstruction Workflow

At the time this study was performed, numerous commercial SfM processing software packages were available for licensing. A preliminary study was performed with a separate dataset of 600 images taken of rock outcrops located in Central/Eastern Utah to evaluate many of these software packages. Ultimately, Agisoft® *PhotoScan v1.1.6 Professional* (Agi) was selected for this study due to its robustness, reasonable price, workflow flexibility, and wide use in the academic literature (Arbués et al. 2012; Kersten and Lindstaedt 2012; Koska and Kremen 2013; Lucieer et al. 2014; Room and Ahmad 2014; Trier et al. 2012; Turner et al. 2015). This software made adjustments for the minor lens distortions in the photos from the camera lenses.

For optimal results, *PhotoScan* requires 60% image overlap for horizontal features, and 80% image overlap for vertical features (Agisoft LLC 2011). Blurred images, reflective surfaces, and/or excessive data outside the area of interest can interfere with accurate scene reconstruction. For consistency and to replicate the likely workflow that an engineer or scientist would apply if using the software, the recommended workflow described in the *PhotoScan* user manual (Agisoft LLC 2011) was incorporated in this study. This workflow can be summarized as follows:

- *Upload Images* - Image sets from each sUAV platform were uploaded to *PhotoScan*.
- *Align Images* - The “Align Photos” function in *PhotoScan* was performed with each image set using the following settings:
 - Accuracy: High
 - Pair Preselection: Disabled

- Point Limit: 4,000,000

During this phase, camera positions and orientations were back-calculated, and a sparse point cloud was developed.

- *Dense Point Cloud Development* - The “Build Dense Cloud” function in *PhotoScan* was performed next for each model with the following settings:
 - Accuracy: High
 - Depth Filtering: Aggressive
- *Point Cloud Export* - The “Export Points” function in *PhotoScan* was then applied with each resulting dense point cloud, generating a .PLY file that could be analyzed in the point cloud manipulation software *CloudCompare* (Girardeau-Nontaut; Tang 2012) and compared with the TLS point cloud model.
- *Point Cloud Scaling* - Using objects of known size and dimensions in the various point cloud models, including the measured distances between highway guardrail posts, the point clouds were scaled to actual dimensions. This step in the workflow is usually not necessary if ground control points are incorporated in the field data collection and the SfM computer vision processing.

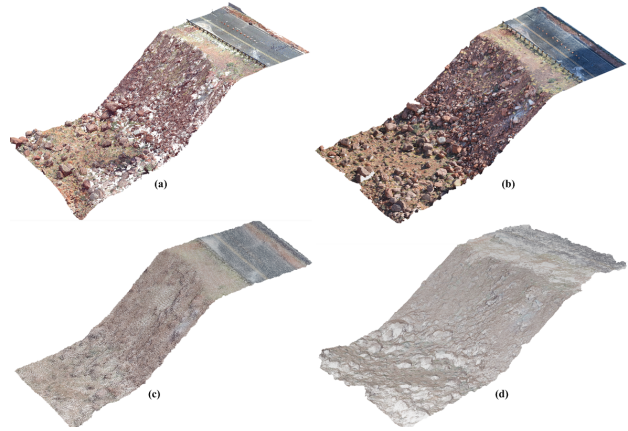
4. Results and Discussion

4.1. Quantitative Results

For consistency between the various 3D models, a section of the landslide that was clearly visible in all 3D models was used to assess model resolution and accuracy. This selected section was located at the front-center of the landslide and was segmented out from each parent model, as shown in Figure 5. The number of points in each segmented section was divided by the computed surface area of the section to calculate the number of points per square meter in the section. To obtain the ground nearest distance (GND) between points, the resolution value was inverted, square rooted and multiplied by 100 to obtain results in units of centimeters/point. The GND therefore represents the average distance (in cm) between points in each model.

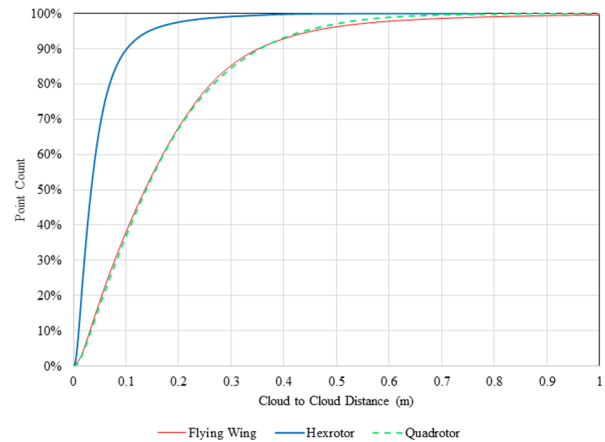
Accuracy assessment between sUAV-based computer vision point clouds and the TLS point cloud was performed using the cloud-to-cloud distance computation function of *CloudCompare* (Girardeau-Nontaut). Using *CloudCompare*, the selected sections from each UAV-based point cloud model were aligned in free space with the corresponding section from the TLS point cloud model using the ICP algorithm. This algorithm lined the models up for comparison using the cloud-to-cloud (C2C) distance function. Although the ICP method will introduce some error into the alignment of the models, this error is insignificant when compared to the errors from inaccuracies in the computer vision point clouds. The *c2c* function computes the average discrepancy between the points of the two models in terms of distance (in meters). In addition, the function also computes the statistical cumulative distribution functions of the C2C average discrepancies, which are shown in Figure 6. From these distribution functions, the median C2C discrepancies are approximately 3.3, 13.8, and 13.7 cm for the Hexrotor

Fig. 5. Sections of the point clouds of the US-89 landslide used to assess model resolution and accuracy. (a) TLS point cloud, (b) Hexrotor / D7100 point cloud, (c) Quadrotor / GoPro point cloud, and (d) Flying Wing / GoPro point cloud.



/ D7100, Quadrotor / GoPro, and Flying Wing / GoPro platform/sensor combinations, respectively. Additionally, Table 3 summarizes the resolution and accuracy results (as compared to the TLS ground truth model), as well as approximate equipment cost and required man-hours for each sUAV/sensor combination evaluated in this study.

Fig. 6. Cumulative distribution plots of the Hexrotor / D7100, Quadrotor / GoPro, and Flying Wing / GoPro models’ C2C discrepancies (in meters) as compared to the TLS ground truth model.



Color-graduated comparisons of the models, developed using *CloudCompare*, are presented in Figures 7 through 9. These models show the C2C discrepancy (in meters) from each point to the closest corresponding point on the TLS point cloud. Each C2C discrepancy value is assigned a color, according to the legend alongside each graph. From these comparisons, it can be seen that the Hexrotor / D7100 platform/sensor combination produced the most resolute and accurate model because the majority of the model is blue, representing a C2C discrepancy of no more than 10 cm. The Quadrotor / GoPro and Flying Wing / GoPro combinations each demonstrate similar C2C discrepancies, with the majority of the points falling within 25 cm

Table 3. Comparison of various slope segment models against TLS ground truth model.

	TLS	Hexrotor & Nikon D7100	Quadrotor & GoPro Hero 3+	Flying Wing & GoPro Hero 3+
Resolution (points/m ²)	90,417	6,919	99	85
GND (cm/point)	0.11	1.2	10	10.8
Median ICP Accuracy Compared to TLS (cm)	N/A	3.3	13.8	13.7
ICP Accuracy Compared to TLS(% within 1 cm of TLS)	N/A	9.80%	1.17%	1.96%
ICP Accuracy Compared to TLS(% within 10 cm of TLS)	N/A	90%	38%	39%
Equipment Cost (Approx.)	\$100,000	\$9,000	\$1,500	\$800
Field Collection Man-Hours	32	2	2	2

of the TLS ground truth model. However, it is obvious that the Flying Wing / GoPro model is less resolute than the Quadrotor / GoPro model due to the fewer number of colored points in the model. Also interesting is the fact that the Flying Wing / GoPro model demonstrated significantly worse accuracy along the pavement surface than the other sUAV-based point cloud models. We suspect that this reduced accuracy along the pavement is due to the image blur from the Flying Wing digital images. This reduced accuracy along the pavement is very apparent in the results from the wooden boxes.

Fig. 7. C2C discrepancy between the Hexrotor / D7100 model to the TLS ground truth model. Median difference between the clouds is approximately 3.3 cm.

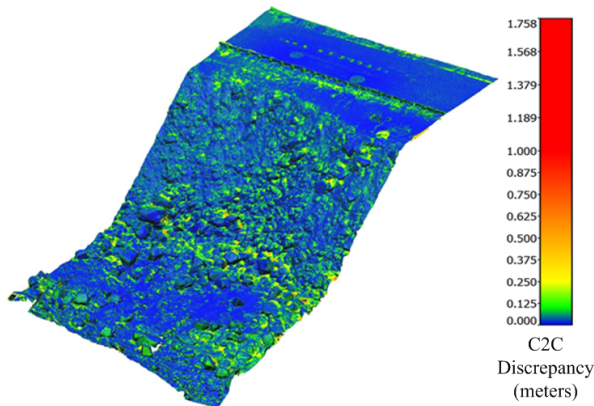


Fig. 8. C2C comparison of the Quadrotor / GoPro model to the TLS ground truth model. Median difference between the clouds is approximately 13.8 cm.

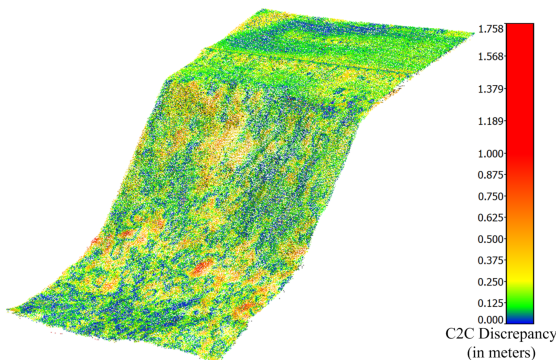
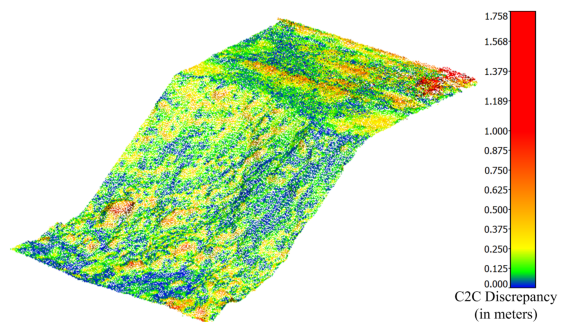


Fig. 9. C2C comparison of the Flying Wing / GoPro model to the TLS ground truth model. Median difference between the clouds is approximately 13.7 cm.



4.1.1. Comparison of Standard Boxes

Comparisons of the box portions of the point cloud models are presented in Figure 10. These comparisons demonstrate the impact that GND has on model clarity. The TLS ground truth model, with a GND of 0.11 cm, clearly shows each individual box. The Hexrotor / D7100 model, with a higher GND of 1.2 cm, also clearly shows the boxes, but is becoming grainier and more difficult to interpret some of the smaller boxes. The Quadrotor / GoPro model appears much grainier, and is difficult to interpret all but the largest of the boxes. Finally, the Flying Wing / GoPro model appears the grainiest, and it is nearly impossible to distinguish any of the boxes.

These comparisons with the wooden boxes are better demonstrated when cross-sections through the boxes from each model are compared against the dense point cloud from the TLS model, as demonstrated in Figure 11. The Hexrotor / D7100 model cross-section of the boxes presented in Figure 11(a) shows the best representation of depth modeling in this experiment. The blue line aligns closely with the TLS model with slight distortion occurring at the corners between the road and the boxes. The Quadrotor / GoPro model cross-section of the boxes presented in Figure 11(b) shows less precision. The cross-section from the model seems to touch the tops of the boxes that were wider than 20 cm horizontally, but did not accurately follow the outline of the boxes back to the roadway surface. Boxes that were skinnier than 20 cm horizontally did not seem to be visible at all in the model. The Flying Wing / GoPro model cross-section of the boxes presented in Figure 11(c) shows the least precision of all of the SfM models, with none of the boxes accurately captured in the model.

Fig. 10. Comparison of 3D point cloud models of the wooden boxes on the US-89 highway from the (a) TLS, (b) Hexrotor / D7100, (c) Quadrotor / GoPro, and (d) Flying Wing / GoPro

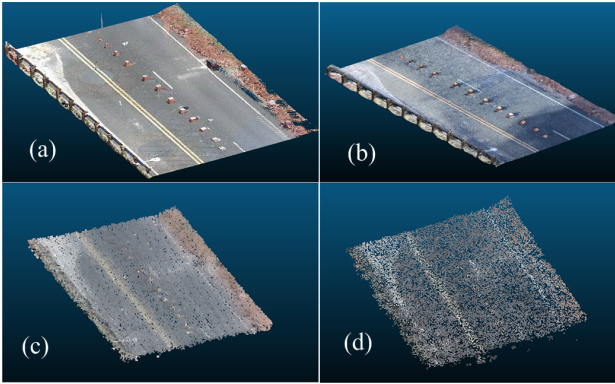


Fig. 11. Comparison of 2D cross sections of the wooden boxes with the ground truth LiDAR on the US-89 highway. The cross sections are shown as colored lines against the LiDAR point cloud.



4.2. Discussion of the Quantitative Results

Much inference can be made by investigating Figures 6-11 and Table 3. Inspection of the point cloud models of the wooden boxes in Figure 10 and the corresponding cross-sections through several of those boxes in Figure 11 reveals that the Hexrotor / D7100 platform/sensor combination was superior in both model resolution and accuracy. This can be attributed to the superior CCD global sensor and higher pixel resolution of the D7100 DSLR camera, as well as the image stabilization technology and improved flight stability of the multi-rotor sUAV platform. However, there is also a noticeable difference in the resolution of the boxes between the Flying Wing / GoPro models and the Quadrotor / GoPro models, as shown in Figures 10 and 11. The Flying Wing / GoPro model has a noticeably inferior resolution despite the fact that both sUAV platforms were carrying the same camera and were flying along similar paths and elevations. Yet, the model accuracies for both the Flying Wing / GoPro and the Quadrotor / GoPro combinations were nearly identical, as shown in Figure 6, Figures 8-9, and Table 3. Thus, any given point in either the Flying Wing / GoPro model or the Quadrotor / GoPro model has approximately the same error in terms of its correct location in space. However, the Quadrotor / GoPro model has more points overall, hence a higher resolution than the Flying Wing / GoPro model. The reason that the Flying Wing / GoPro model has fewer points is likely due to pixel blur in the images from the higher velocity of the Flying Wing, as well as a lack of on-board sensor stabilization technology, resulting in an inferior 3D reconstruction.

In terms of the two questions that were initially posed for this study, these results suggest that camera selection is perhaps the most important consideration in determining a point cloud model's resolution and accuracy. The selection of the sUAV platform is also important in two regards. First, the platform must be capable of carrying the selected camera and any additional image stabilization technology that is desired. Second, the platform must be capable of flying in the manner necessary to collect images of sufficient quality for the desired 3D reconstruction. sUAV platforms flying at a higher velocity will have a greater risk of experiencing pixel blur, which will impact the resolution of the resulting point cloud model. Flying at higher elevations will decrease the propensity for pixel blur, but will also increase the GSD of the images, and subsequently reduce the resolution of the 3D reconstruction.

4.3. Qualitative Results

The qualitative appearance of a 3D model is very important for many applications, though it is often difficult to objectively quantify. For example, excessive gaps and holes in a model that is otherwise highly accurate can limit the model's usefulness. Some applications, such as anomaly detection, virtual visual inspection, and presentation for marketing or business development can actually rely more on qualitative appearance than on precise model measurements. Therefore, a subjective qualitative assessment was performed for each of the 3D reconstructions developed in this study.

4.3.1. Terrestrial Laser Scan

The TLS model, as presented in Figure 3, effectively displays the survey area, with very sharp, easy to identify details. Even the smallest wooden box is reconstructed with well-defined edges that are easily visible and accurately measurable in *CloudCompare*. Vegetation in the TLS model is clearly visible, with size, shape, color, and some texture of vegetation generally observable in the model. Road markings and color variations on rocks are accurately reproduced. However, a significant number of "holes" are present in the TLS model due to the numerous occlusions at the site that limited the line of sight of the TLS scanners. These holes were estimated to be 7% of the surface area. This was estimated by creating a mesh of the surface, sampling points from the mesh and then counting the points with a cloud to cloud distance greater than 2 standard deviations more than the average GND of the original point cloud. Despite relocating the scanners to 16 different scan points across the landslide, shadow zones in the model are still readily abundant. The areas where the scanners could effectively and safely be placed were limited by the steepness and ruggedness of the terrain. As a result, many objects in the model, particularly the mid-sized boulders and bushes, appear incomplete in the model. While we acknowledge that shadow zones can generally be overcome by operating the TLS from more positions, such effort can dramatically increase the time and costs associated with data collection.

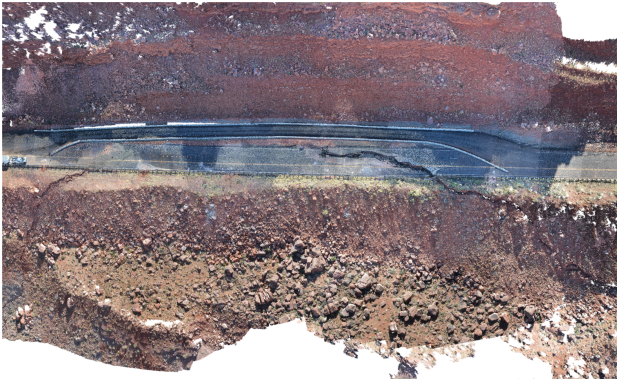
4.3.2. Hexrotor / D7100 Model

An image of the Hexrotor / D7100 point cloud model is presented in Figure 12. The model shows very good qualitative results. Size, geometry, and color are all clearly distinguishable on most objects in the model. Not many holes or incomplete

objects are visible. The holes in this model were estimated to be 0.5% of the model surface area. Significantly better than the 7% for the TLS model. The relatively high density of points in the point cloud allows for high-resolution model detail and clear object interpretation without need of additional meshing or texturing. All of the wooden boxes are visible and distinct, although their geometry is heavily rounded at the corners and edges, as was shown in Figure 11. Vegetation is generally visible in the model, and size and color can be estimated relatively easily. However, texture of the vegetation is neither clear nor definable, and the geometry of the vegetation produces a curved and blended appearance. Road markings and color variations on rocks are accurately reproduced. Shadowed objects are visible in the point cloud, and do not appear to negatively impact the overall quality of the model.

The most significant qualitative drawback of the Hexrotor / D7100 model is the curvature of edged objects. This rounding effect was observed on many of the rocks and boulders in the model. The edges and sharp features of these objects remain readily visible, but are softened considerably in the point cloud. Improved image resolution, overlap, and/or computer processing capabilities would likely produce a higher point cloud resolution and accuracy, thus reducing this rounding effect.

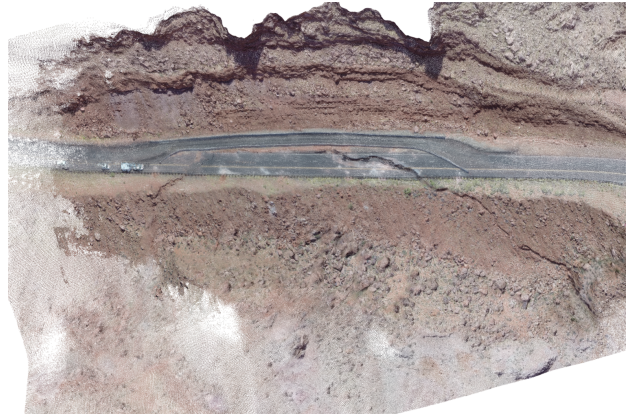
Fig. 12. Hexrotor / D7100 3D reconstruction of the US-89 landslide.



4.3.3. Quadrotor / GoPro Model

An image of the Quadrotor / GoPro model is presented in Figure 13. There is a noticeable decrease in the resolution of the Quadrotor / GoPro model that is roughly proportional to the reduced resolution of the still images used in the SfM reconstruction. This reduced resolution produces a much grainier point cloud appearance, as observed in Figure 10, but with relatively few holes or discontinuities. The box edges are severely rounded and not readily visible (see Figure 11). Vegetation remains visible in the Quadrotor / GoPro model, but is generally indistinguishable from the surrounding rocks if it were not for the color of the points. Road markings and color variations on rocks remain somewhat visible and identifiable, but are quite blurred. Rocks are generally distinguished by their size, color, and location, but the geometry of individual rocks is difficult to distinguish. Shadowed objects remain visible, but are less defined.

Fig. 13. Quadrotor / GoPro 3D point cloud model of the US-89 landslide.



4.3.4. Flying Wing / GoPro Model

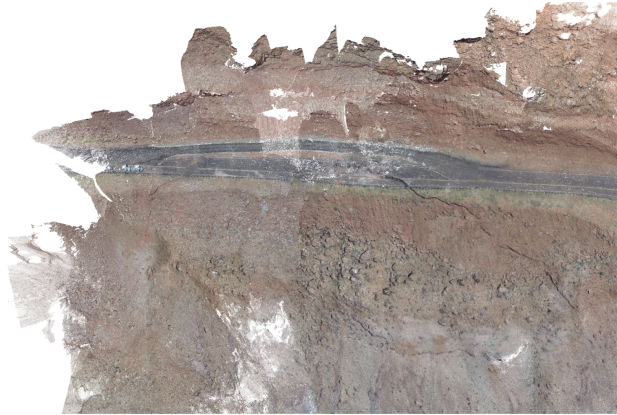
An image of the Flying Wing / GoPro model is presented in Figure 14. The resolution of the Flying Wing / GoPro model is slightly worse than the resolution of the Quadrotor / GoPro model. Qualitatively, the two GoPro models have similar features, except that the Flying Wing / GoPro model is much more blurred and grainy, as can be seen in Figure 10. This is due to the lack of any image stabilization technology on the fixed wing sUAV and the slightly higher ground velocities that the fixed wing was flown at. Cross-sections of the wooden boxes appeared in the Flying Wing / GoPro model did not accurately represent the boxes (see Figure 11). None of the wooden boxes are clearly visible in the 3D reconstruction. Vegetation and road markings are still visible in the Flying Wing / GoPro model, but are much more blurred than in the Quadrotor / GoPro model. Some color variation on a few of the boulders is visible, but only the larger boulders can be individually distinguished in the 3D reconstruction. Shadowed objects remain visible in the Flying Wing / GoPro model, but are very blurred.

The most attractive qualitative feature of the Flying Wing / GoPro model is that it covers the largest geographic area of any of the models that were developed. This could be due to the fact that the flying wing sUAV has a much larger turn radius than its multi-rotor counterparts, and can cover much more area than a multi-rotor in a given amount of time due to its increased flight velocity.

4.4. Additional Considerations and Practical Guidance for Engineers/Scientists

While the Quadrotor / GoPro and Flying Wing / GoPro models have a much lower resolution and accuracy than either the TLS or the Hexrotor / D7100 models, they should not necessarily be labeled as “inferior” without a consideration of their intended purpose or objective. For example, even though the TLS and Hexrotor / D7100 models have excellent resolution, their file sizes (13GB and 3GB, respectively) are relatively large, thus making them bulky, difficult to distribute/share, and generally limited to use on specialized workstation computers that have the necessary hardware to view and manipulate them. Conversely, the Quadrotor / GoPro and Flying Wing / GoPro models are much smaller in file size (0.5GB and 0.3GB, respectively), making them easier to distribute/share and more

Fig. 14. Flying Wing / GoPro 3D point cloud model of the US-89 landslide.



viewable/usable on a wider range of computers and workstations. If an engineer or scientist wanted to make accurate measurements (change detection analysis) with the point cloud models, then he/she would likely want a high-resolution point cloud such as the TLS or Hexrotor / D7100 model. However, if the engineer or scientist simply wanted to create a 3D visualization of a particular site for qualitative or marketing/presentation purposes, and did not require accurate measurements or change detection from the model, then the lower-resolution Quadrotor / GoPro or Flying Wing / GoPro models would likely be superior. The lower-resolution modeling solutions may even be more appealing to engineers and scientists when they consider that the Quadrotor / GoPro and Flying Wing / GoPro platform/sensor combinations generally cost significantly less than the heavy-lift multi-rotor/DSLR platform/sensor combinations, and are generally much easier to operate, maintain and transport.

The ideal platform/sensor combination for remote sensing with SfM computer vision depends upon several variable factors including: (1) desired model resolution and accuracy, (2) the potential need for quantitative or qualitative model assessments, (3) the size of the area to be modeled, (4) the level of sUAV operator experience and skill, (5) the operating environment (high winds, extreme temperatures, inhibitive infrastructure such as overhead power lines), (6) the ability to obtain necessary federal and local authorizations to operate sUAVs commercially, and (7) the funds available for the necessary sUAV and sensor hardware acquisition. Each possible sUAV/sensor combination has varying advantages and disadvantages related to these identified factors, and should be carefully considered by an engineer or scientist prior to equipment acquisition and operation.

As demonstrated in this study, resolution and accuracy are primarily affected by the resolution and image sensor quality of the selected digital camera, the quality of imaging lens, the altitude and velocity of the sUAV, and the availability/effectiveness of image stabilization technology (self-adjusting multi-axis gimbal). High-resolution DSLR cameras are excellent optical sensors for UAV-based remote sensing with SfM computer vision, but require larger and more expensive sUAV platforms that are capable of carrying larger payloads for a sufficient flight duration. Alternatively, smaller digital cameras (point-and-shoot cameras or durable sports cameras such as a GoPro) can be

carried by the majority of sUAV platforms that are currently commercially available, but generally result in poorer model resolution and accuracy due to their reduced image resolution and/or inferior image sensor. UAV platform specifications must be carefully reviewed to ensure sufficient payload capacity and/or flight duration to carry the chosen sensor and all necessary accessories (sensor gimbals and controllers) to complete the desired remote sensing mission(s).

The desired engineering or scientific application should drive the selection of the sUAV/sensor combination accordingly. For engineering or scientific applications where small (< 10 cm) displacements or deformations must be detected and measured, or where small object details must be captured in the 3D reconstruction, a heavy-lift multi- or single-rotor sUAV platform and DSLR camera combination with image stabilization technology would likely be required. A smaller sUAV (small quadrotor or fixed wing) and digital camera combination is recommended for applications that can tolerate model inaccuracies of up to approximately 50 cm, require faster model processing times, and/or require wider aerial coverage. Any engineering application that requires a high level of model detail on vertical surfaces or an sUAV flight in a constrained environment should incorporate a multi- or single-rotor sUAV platform that is capable of hovering and vertical flight instead of a fixed wing sUAV platform.

Engineers and scientists must also consider site conditions in addition to desired model resolution/accuracy when selecting a particular sUAV/sensor combination for remote sensing applications. Wind, temperature, and site obstacles can all influence the ability of a particular sUAV platform to perform adequately. For example, our Hexrotor sUAV platform could only be flown before 10:00 AM at the US-89 landslide because the hot temperatures later in the day were causing the platform to malfunction and/or fail because some heavy-lift multi-rotor sUAV platforms rely upon controller modules that are relatively sensitive to temperature. For extreme temperature conditions, single-rotor or fixed wing sUAV platforms generally are much more resilient, but require greater skill and experience to operate. As another example, multi-rotor sUAV platforms generally perform very well in cluttered environments due to their superior maneuverability (assuming skilled sUAV operators are controlling the platforms). However, these same multi-rotor sUAV platforms generally perform quite poorly in windy environments (gusts in excess of 30 km per hour based on our experience), and can experience dramatically increased power consumption and operator workload to maintain flight path and aerial stability. In such windy environments, fixed wing and/or single-rotor sUAV platforms are generally much more reliable in flight. However, these types of sUAV platforms can be much more difficult to operate, and may require a more seasoned and experienced sUAV operator. Matching pilot skill and experience to the sUAV platform and environmental conditions are absolutely essential for safety, loss prevention, and quality data collection (Stark et al. 2012).

5. Conclusions and Recommendations

To assess the effect of the sUAV platform on the resolution and accuracy of UAV-based remote sensing with SfM computer vision, three different sUAV/sensor combination were

tested to produce 3D reconstructions of a section of US Highway 89 near Page, Arizona that had experienced significant damage due to a 2013 landslide. Imagery used to build the three 3D reconstructions were collected using the following sUAV/sensor combinations: a heavy-lift Skyjib Hexrotor sUAV carrying a Nikon D7100 DSLR camera, a DJI Phantom II Quadrotor sUAV carrying a GoPro Hero 3+ camera with customized 5.4mm flat lens, and an 208-cm Ritewing fixed wing sUAV also carrying a GoPro Hero 3+ camera with customized 5.4mm flat lens. A baseline 3D reconstruction of the landslide was created with two different terrestrial laser scanner (TLS) devices: a FARO Focus^{3D} 130 and a FARO Focus^{3D} 330. TLS data was processed with AutoDesk ReCap software, and the SfM computer vision processing was performed with Agisoft *PhotoScan*. Resolution of each sUAV-based 3D reconstruction was manually calculated, and accuracy of each 3D reconstruction was quantified by comparison with the baseline model using ICP analysis with the software *CloudCompare*. Qualitative evaluations were also performed and documented visually by the authors.

The largest factor affecting both accuracy and resolution, or quantitative results of the aerial models was the camera resolution. The 24 MP images captured with the Nikon D7100 camera generated a model resolution about 70 times greater than that from the 2.76 MP images taken from the GoPro Hero 3+ camera. The Nikon D7100 model was also about 4 times more accurate on average than the GoPro Hero 3+ models when compared against the TLS ground-truth model using ICP analysis. However, we observed that the sUAV platform selection also had a significant impact on the resolution of the point cloud model, with a 16% increase in point resolution when a multi-rotor platform with sensor stabilization technology was used instead of a fixed wing platform without sensor stabilization technology.

Additional observations and guidance from this study include the following:

- The intended application and the necessary resolution and accuracy of the 3D point cloud model is the most important factor to consider when selecting an sUAV platform and corresponding imaging sensor
- Still imagery generally produces superior SfM 3D reconstructions to images that have been extracted from video
- sUAV platform selection will be limited by sensor weight
- Fixed wing and single-rotor platforms cover larger areas and are more robust in extreme environments that are prone to drastic changes in temperature, but are more susceptible to motion blur in the collected imagery unless they incorporate some type of image stabilization technology
- Multi-rotor sUAV platforms collect high-quality imagery with minimal motion blur, and are desirable for applications requiring resolute and accurate models, but tend to be more negatively impacted by environmental factors like wind and extreme temperatures

- The sUAV platform selected must be compatible with the skill level of the intended operator and the anticipated environmental conditions to ensure safety and minimize platform damage
- There are cost, weight, size and operational tradeoffs for platform/sensor combinations to achieve the accuracy required for an intended mission

Because related technologies are rapidly expanding, the best practices for performing sUAV-based remote sensing with SfM computer vision will continuously evolve and improve. However, the results and guidance presented by this study will provide some useful basis for development of general principles of operation for engineers and scientists desiring to use sUAV-based remote sensing to collect data from the field.

Acknowledgments

Funding for this study was provided by the National Science Foundation's Industry/University Cooperative Research Center for Unmanned Aerial Systems (C-UAS) through project BYU 13-03, and is gratefully acknowledged. Additional material assistance was provided by the Brigham Young University MAGICC lab. Flights were performed by Brandon Reimschuessel and Tim Price.

Software and technical support from Agisoft and Daniel Girardeau -Montaut was instrumental in the completion of this study. The authors would also like to thank Professors Daniel Ames and Gustavious Williams from Brigham Young University for their initial reviews and comments on this paper.

Site access and risk management was provided by the Arizona Department of Transportation and Navajo Nation. TLS survey was performed by Vernon Jensen of AEC 3D Laser Scanning of Cypress, CA. Geotechnical information from the US-89 landslide was collected and made available by Kleinfelder, Inc. Technical support and advice was provided by both AEC 3D Laser Scanning and Meridian Engineering of Salt Lake City, UT. This support and collaboration is gratefully acknowledged.

Author Contributions

Kevin Franke, Joseph Clark, Abraham Martin, and John Heden- gren conceived and designed the experiments and the study. Kevin Franke, Joseph Clark, and Brandon Reimschuessel performed the sUAV experiments and collected the data. Joseph Clark and Abraham Martin processed, analyzed and interpreted the data. Samantha Ruggles, Joseph Clark, Kevin Franke, Derek Wolfe, Trent Okeson, and Abraham Martin drafted the paper. All authors read and edited drafts, and approved the final manuscript.

References

- Agisoft PhotoScan. <http://www.agisoft.com/>. Accessed: 2015-12-21.
- Reality capture and 3D scanning software. <http://www.autodesk.com/products/recap/overview>. Accessed: 2015-12-21.

- Agisoft LLC, 2011. Agisoft PhotoScan User Manual. Technical report.
- Arbués, Pau, Garcia, David, Granado, Pablo, and Muñoz, Josep Anton, 2012. A Method for Producing Photorealistic Digital Outcrop Models. 74th EAGE Conference & Exhibition incorporating SPE EUROPEC 2012 Copenhagen, Denmark, 4-7 June 2012 (June 2012): 4–7.
- Bemis, Sean P, Micklethwaite, Steven, Turner, Darren, James, Mike R, Akciz, Sinan, Thiele, Sam T, and Bangash, Hasnain Ali, 2014. Ground-based and UAV-Based photogrammetry: A multi-scale, high-resolution mapping tool for structural geology and paleoseismology. *Journal of Structural Geology* **69**: 163–178.
- Besl, Paul J and McKay, Neil D, 1992. Method for registration of 3-D shapes. In *Robotics-DL tentative*, 586–606. International Society for Optics and Photonics.
- Coifman, B, McCord, M, Mishalani, RG, Iswalt, M, and Ji, Yuxiong, 2006. Roadway traffic monitoring from an unmanned aerial vehicle. In *IEE Proceedings-Intelligent Transport Systems*, volume 153, 11–20. IET.
- Coopmans, Calvin, 2014. Architecture requirements for ethical, accurate, and resilient unmanned aerial personal remote sensing. doi:10.1109/ICUAS.2014.6842233.
- de Albuquerque Nóbrega, Rodrigo Affonso, Aanstoos, James, Gokaraju, Balakrishna, Mahrooghy, Majid, Dabirru, Lalitha, and O'Hara, Charles G, 2013. Mapping weaknesses in the Mississippi river levee system using multi-temporal UAVSAR data. *Revista Brasileira de Cartografia* (65/4).
- Dobson, Richard J., Brooks, Colin, Roussi, Chris, and Colling, Tim, 2013. Developing an unpaved road assessment system for practical deployment with high-resolution optical data collection using a helicopter UAV. 2013 International Conference on Unmanned Aircraft Systems, ICUAS 2013 - Conference Proceedings 235–243. doi: 10.1109/ICUAS.2013.6564695.
- D'Oleire-Oltmanns, Sebastian, Marzloff, Irene, Peter, Klaus, and Ries, Johannes, 2012. Unmanned Aerial Vehicle (UAV) for Monitoring Soil Erosion in Morocco. *Remote Sensing* **4** (12): 3390–3416. doi:10.3390/rs4113390.
- Girardeau-Nontaut, Daniel. CloudCompare.
- Gong, Jianhua, Wang, Dongchuan, Li, Yi, Zhang, Lihui, Yue, Yujuan, Zhou, Jieping, and Song, Yiquan, 2010. Earthquake-induced geological hazards detection under hierarchical stripping classification framework in the Beichuan area. *Landslides* **7** (2): 181–189.
- Harwin, Steve and Lucieer, Arko, 2012. Assessing the accuracy of georeferenced point clouds produced via multi-view stereopsis from Unmanned Aerial Vehicle (UAV) imagery. doi:10.3390/rs4061573.
- Hausamann, Dieter, Zirinig, Werner, Schreier, Gunter, and Strobl, Peter, 2005. Monitoring of gas pipelines-a civil UAV application. *Aircraft Engineering and Aerospace Technology* **77** (5): 352–360.
- Hu, Ji Ping, Wu, Wen Bin, and Tan, Qu Lin, 2012. Application of Unmanned Aerial Vehicle Remote Sensing for Geological Disaster Reconnaissance along Transportation Lines: A Case Study. In *Applied Mechanics and Materials*, volume 226, 2376–2379. Trans Tech Publ.
- Kaiser, Andreas, Neugirg, Fabian, Rock, Gilles, Müller, Christoph, Haas, Florian, Ries, Johannes, and Schmidt, Jürgen, 2014. Small-scale surface reconstruction and volume calculation of soil erosion in complex Moroccan gully morphology using structure from motion. *Remote Sensing* **6** (8): 7050–7080.
- Kersten, Thomas P. and Lindstaedt, Maren, 2012. Image-based low-cost systems for automatic 3D recording and modelling of archaeological finds and objects. *Lecture Notes in Computer Science (including subseries Lecture Notes in Artificial Intelligence and Lecture Notes in Bioinformatics)* **7616 LNCS**: 1–10. doi:10.1007/978-3-642-34234-9_1.
- Koska, B and Kremen, T., 2013. The Combination of Laser Scanning and Structure from Motion Technology for Creation of Accurate Exterior and Interior Orthophotos of St. Nicholas Baroque Chrich. *International Archives of Photogrammetry, Remote Sensing and Spatial Information Sciences*, **XL** (February): 25–26.
- Ledezma, Christian, 2014. *Geotechnical aspects of April 1, 2014, M8.2 Iquique, Chile earthquake*. Ph.D. thesis, Pontificia Universidad Católica de Chile.
- Lucieer, a., Jong, S. M. D., and Turner, D., 2014. Mapping landslide displacements using Structure from Motion (SfM) and image correlation of multi-temporal UAV photography. doi:10.1177/0309133313515293.
- Mancini, Francesco, Dubbini, Marco, Gattelli, Mario, Stecchi, Francesco, Fabbri, Stefano, and Gabbianelli, Giovanni, 2013. Using unmanned aerial vehicles (UAV) for high-resolution reconstruction of topography: The structure from motion approach on coastal environments. doi: 10.3390/rs5126880.
- Marr, David and Nishihara, Herbert Keith, 1978. Representation and recognition of the spatial organization of three-dimensional shapes. *Proceedings of the Royal Society of London B: Biological Sciences* **200** (1140): 269–294.
- McCormick, William V. and Richmond, Jeff C., 2013. *Geotechnical Assessment, Bitter Springs Landslide, US Highway 89*. Technical report, Kleinfelder West, Tempe, AZ.
- Metni, Najib and Hamel, Tarek, 2007. A UAV for bridge inspection: Visual servoing control law with orientation limits. *Automation in construction* **17** (1): 3–10.
- Niethammer, U., James, M. R., Rothmund, S., Tranelletti, J., and Joswig, M., 2012. UAV-based remote sensing of the Super-Sauze landslide: Evaluation and results. doi: 10.1016/j.enggeo.2011.03.012.

- Rathinam, Sivakumar, Kim, Zu Whan, and Sengupta, Raja, 2008. Vision-based monitoring of locally linear structures using an unmanned aerial vehicle 1. *Journal of Infrastructure Systems* **14** (1): 52–63.
- Room, M H M and Ahmad, a, 2014. Mapping of a river using close range photogrammetry technique and unmanned aerial vehicle system. *IOP Conference Series: Earth and Environmental Science* **18**: 012061. doi:10.1088/1755-1315/18/1/012061.
- Siebert, Sebastian and Teizer, Jochen, 2014. Mobile 3D mapping for surveying earthwork projects using an Unmanned Aerial Vehicle (UAV) system. *Automation in Construction* **41**: 1–14.
- Snaveley, Noah, Seitz, Steven M, and Szeliski, Richard, 2008. Modeling the world from internet photo collections. *International Journal of Computer Vision* **80** (2): 189–210.
- Stark, Brandon, Coopmans, Calvin, and Chen, Yangquan, 2012. A framework for analyzing human factors in unmanned aerial systems. *Proceedings - 2012 5th International Symposium on Resilient Control Systems, ISRCS 2012* 13–18. doi:10.1109/ISRCS.2012.6309286.
- Stefanik, Kevin V, Gassaway, Jason C, Kochersberger, Kevin, and Abbott, A Lynn, 2011. UAV-based stereo vision for rapid aerial terrain mapping. *GIScience & Remote Sensing* **48** (1): 24–49.
- Stumpf, André, Malet, Jean-Philippe, Kerle, Norman, Niethammer, Uwe, and Rothmund, Sabrina, 2013. Image-based mapping of surface fissures for the investigation of landslide dynamics. *Geomorphology* **186**: 12–27.
- Tang, Pingbo; Fahd Saleh Alaswad, 2012. Sensor Modeling of Laser Scanner for Automated Scan Planning on Construction Jobsites. *ASCE Library* 1–10.
- Travelletti, J., Delacourt, C., Allemand, P., Malet, J. P., Schmitzbühl, J., Toussaint, R., and Bastard, M., 2012. Correlation of multi-temporal ground-based optical images for landslide monitoring: Application, potential and limitations. doi: 10.1016/j.isprsjprs.2012.03.007.
- Trier, Øivind Due, Pilø, and Holger, Lars, 2012. Automatic Detection of Pit Structures in Airborne Laser Scanning Data. *Archaeological Prospection* **19** (2): 103–121. doi: 10.1002/arp.
- Turner, Darren, Lucieer, Arko, and de Jong, Steven M, 2015. Time series analysis of landslide dynamics using an unmanned aerial vehicle (UAV). *Remote Sensing* **7** (2): 1736–1757.
- Zhang, Chunsun and Elaksher, Ahmed, 2012. An Unmanned Aerial Vehicle-Based Imaging System for 3D Measurement of Unpaved Road Surface Distresses1. *Computer-Aided Civil and Infrastructure Engineering* **27** (2): 118–129.
- Zhou, Hailing, Kong, Hui, Wei, Lei, Creighton, Douglas, and Nahavandi, Saeid, 2015. Efficient road detection and tracking for unmanned aerial vehicle. *Intelligent Transportation Systems, IEEE Transactions on* **16** (1): 297–309.